

See discussions, stats, and author profiles for this publication at: <https://www.researchgate.net/publication/273381680>

Two-Dimensionally Extended π -Conjugation of Donor–Acceptor Copolymers via Oligothienyl Side Chains for Efficient Polymer Solar Cells

ARTICLE in MACROMOLECULES · MARCH 2015

Impact Factor: 5.8 · DOI: 10.1021/acs.macromol.5b00056

CITATIONS

3

READS

44

8 AUTHORS, INCLUDING:



Jaewon Lee

Pohang University of Science and Technology

13 PUBLICATIONS 58 CITATIONS

[SEE PROFILE](#)

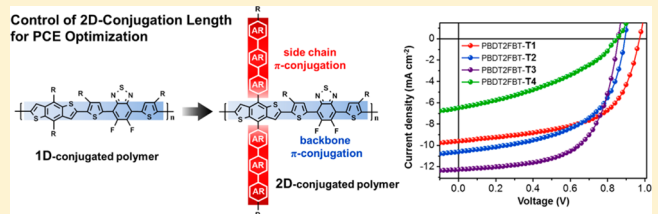
Two-Dimensionally Extended π -Conjugation of Donor–Acceptor Copolymers via Oligothienyl Side Chains for Efficient Polymer Solar Cells

Jaewon Lee,[†] Joo-Hyun Kim,[†] Byungho Moon, Heung Gyu Kim, Min Kim, Jisoo Shin, Hyeongjin Hwang, and Kilwon Cho^{*}

Department of Chemical Engineering, Pohang University of Science and Technology, Pohang, 790-784, Korea

 Supporting Information

ABSTRACT: A series of two-dimensional conjugated polymers containing π -conjugated oligothienyl side chains, namely PBDT2FBT-T1, PBDT2FBT-T2, PBDT2FBT-T3, and PBDT2FBT-T4, was designed and synthesized to investigate the effect of two-dimensionally extended π -conjugation on the polymer solar cell (PSC) performance. The oligothienyl units introduced into the side chains significantly affect the optoelectronic properties of the parent polymers as well as the performances of the resulting solar cell devices by altering the molecular arrangement and packing, crystalline behavior, and microstructure of the polymer:PC₇₁BM blend films. The crystallinity and blend morphology of the polymers can be systematically controlled by tuning the π -conjugation length of side chains; PBDT2FBT-T3 exhibited the most extended UV/vis light absorption band and the highest charge mobility, leading to a high short-circuit current density up to 12.5 mA cm⁻² in the relevant PSCs. The PBDT2FBT-T3:PC₇₁BM-based PSC exhibited the best power conversion efficiency of 6.48% among this series of polymers prepared without the use of processing additives or post-treatments. These results provide a new possibility and valuable insight into the development of efficient medium-bandgap polymers for use in organic solar cells.



1. INTRODUCTION

Over the past decade, polymer solar cells (PSCs) have attracted significant attention due to their predominant advantages of low-cost, lightweight, large-area, flexible, and environmentally friendly energy-converting devices.^{1–3} Tremendous efforts have been devoted toward improving the power conversion efficiencies (PCEs) of bulk-heterojunction (BHJ) solar cells by developing new photoactive polymers. The PCEs of single-junction PSCs now exceed 10.0%.^{4–8} So far, much work has been done to rationalize the energy levels and bandgaps of donor polymers in an effort to maximize photovoltaic efficiency.⁹ Donor–acceptor (D–A) type alternating conjugated polymers have recently been identified as highly promising donor materials for use in future PSCs because the energy levels and bandgaps are tunable via intramolecular charge transfer (ICT) effects.¹⁰

The molecular design of two-dimensional (2D) conjugated polymers presents a promising strategy for improving the PCEs of PSCs based on the formation of extended π -conjugated side chains.^{11–15} Recently, several research groups demonstrated that 2D conjugated polymers with 2-alkylthienyl groups exhibited broader absorption bands, higher hole mobilities, and better photovoltaic properties compared to their alkoxy substituted analogues. For example, benzo[1,2-*b*:4,5-*b'*]-dithiophene (BDT)-based units have largely been utilized to produce 2D conjugated polymers with a variety of side chains including alkyl–phenyl, alkyl–thienyl, alkyl–selenophenyl,

alkyl–thieno[3,2-*b*]thienyl, and alkyl–thienylenevinylenthienyl groups.^{16–23} The π -conjugated side chains efficiently increased the electron density and interchain aggregation among conjugated polymers, thereby enhancing light absorption and charge transport properties of the related PSCs. Moreover, the BDT-based 2D conjugated polymers showed a weak electron-donating property because the thienyl plane was twisted with respect to the BDT plane, providing a low-lying HOMO level that improved the open-circuit voltage (V_{oc}).

Recently, there are a few reports on attempts of introducing oligothienyl side chains to further extend the 2D conjugation lengths of conjugated copolymer systems.^{17–27} The design strategy of extended 2D conjugation described above was used to improve the light absorption properties of donor polymers with only small effects on the molecular energy levels; however, these studies did not achieve improved device performances, probably due to the presence of oversized conjugated side chains that can disrupt backbone coplanarity, thereby decreasing the conjugation length and chain packing in the polymer system.²⁸ Thus, it remains a challenge to develop new molecular design strategies to evolve toward optimizing the physical, chemical, and optoelectronic properties of 2D

Received: January 9, 2015

Revised: February 17, 2015

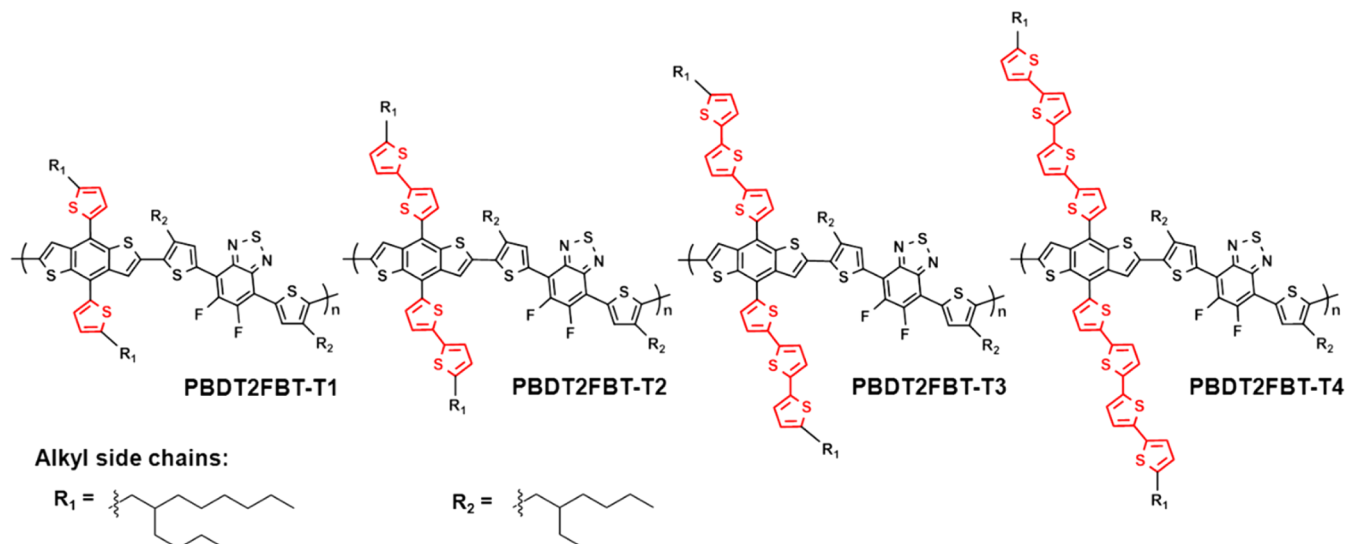
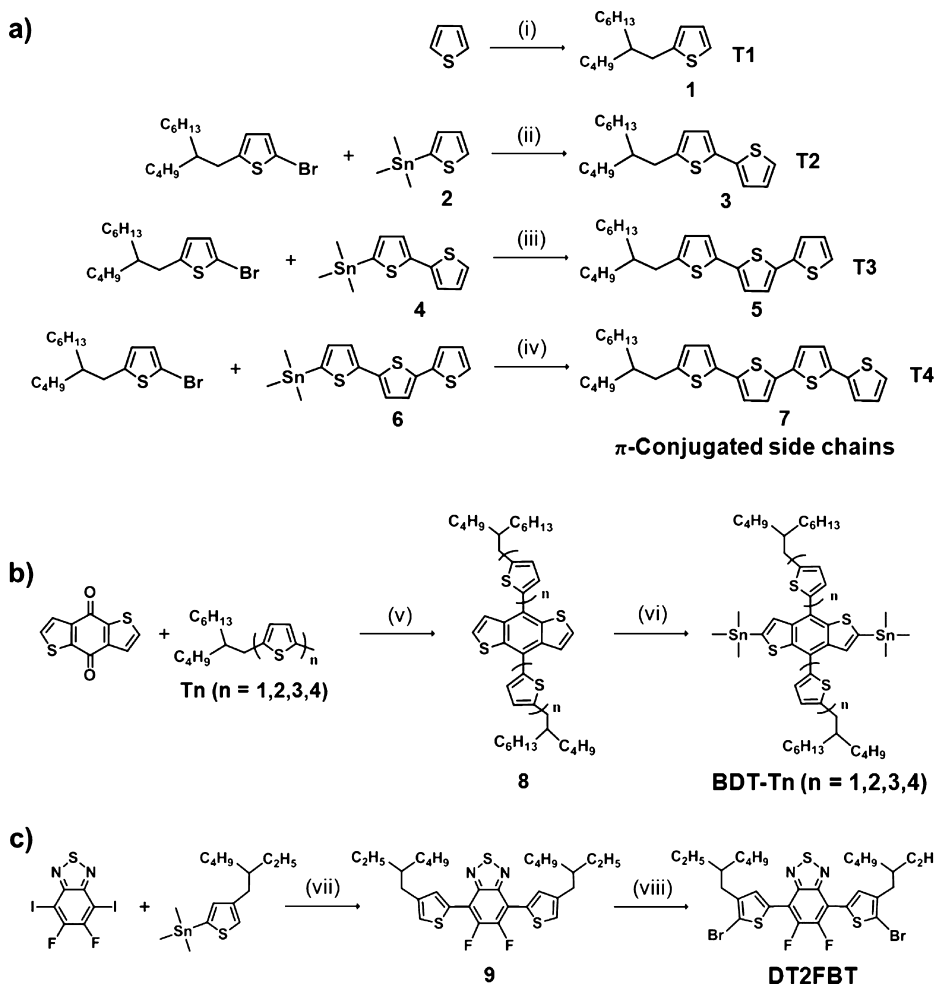


Figure 1. Molecular design of extended 2D-conjugated polymers.

Scheme 1. (a) Synthesis of Oligothienyl Side Chains, T1, T2, T3, and T4,^a (b) Synthesis of Electron Donating Monomers, BDT-T_n^b, and (c) Synthesis of Electron Withdrawing Monomer, DT2FB^cT



^aKey: (i) n-Butyl lithium, NaCl, THF, 55 °C, 6 h; (ii), (iii), and (iv) Pd(PPh₃)₄, toluene/DMF, 105 °C, 48 h. ^bKey: (v) n-butyl lithium, SnCl₂·2H₂O, THF, 55 °C, 6 h; (vi) n-Butyl lithium, trimethyltin chloride, THF, -75 °C, overnight. ^cKey: (vii) Pd(PPh₃)₄, (4-(2-ethylhexyl)thiophen-2-yl)trimethylstannane, toluene, 105 °C, 48 h; (viii) NBS, THF, room temperature, overnight.

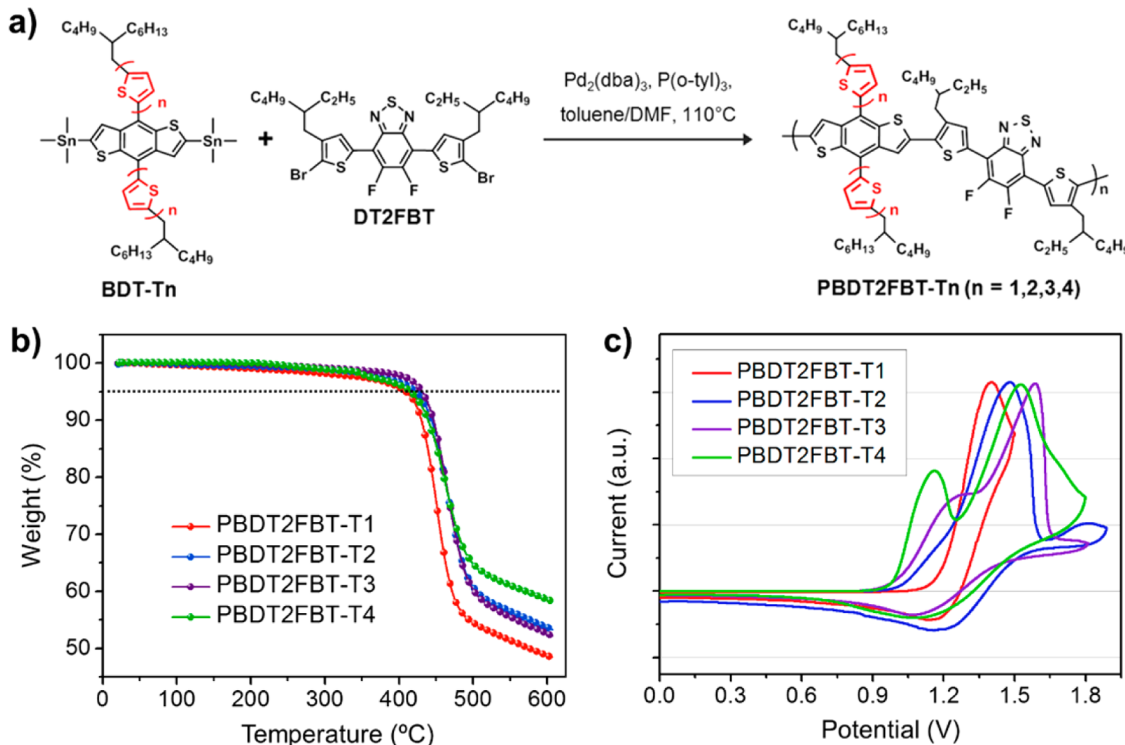


Figure 2. (a) Synthetic procedure of PBDT2FBT-T n 2D-conjugated polymers. (b) TGA plots of PBDT2FBT-T n polymers with a heating rate of 10 $^{\circ}\text{C}$ min $^{-1}$ under an inert atmosphere. (c) Cyclic voltammograms of PBDT2FBT-T n polymers in the CH₃CN solution at a scan rate of 50 mV s $^{-1}$.

Table 1. Molecular Weights, Thermal Properties, and Solubility of PBDT2FBT-T n

polymer	\overline{M}_n (kDa) ^a	\overline{M}_w (kDa) ^a	PDI ^a	T _d ($^{\circ}\text{C}$) ^b	solubility (g L $^{-1}$) ^c
PBDT2FBT-T1	28.1	49.3	1.75	409	34.3
PBDT2FBT-T2	42.8	48.6	1.13	422	20.1
PBDT2FBT-T3	48.2	102.1	2.11	432	22.6
PBDT2FBT-T4	33.8	109.5	3.24	414	28.7

^aDetermined by GPC using polystyrene standards and chlorobenzene (CB) as an eluent. ^b5% weight loss temperatures measured by TGA under nitrogen atmosphere. ^cThe concentration of the saturated solution in 1,2-dichlorobenzene (DCB) at 25 $^{\circ}\text{C}$ according to the Beer–Lambert law.

conjugated polymers that could be useful in high-efficiency PSCs.

On the basis of these considerations, here we report a synthetic strategy for preparing 2D conjugated polymers by introducing π -conjugated thienyl side chains, i.e., alkyl-oligothienyl groups, into benzodithiophene–difluorobenzothiadiazole (BDT-2FBT) copolymers (Figure 1). A series of four medium-bandgap polymers was synthesized by incorporating alkylated thienyl-, bithienyl-, terthienyl-, or quaterthienyl side chains (namely PBDT2FBT-T1, -T2, -T3, and -T4). This series was used to systematically investigate the effects of extended π -conjugation on the key parameters that determine the PCE. The optical, morphological, and photovoltaic properties of the PSCs were evaluated based on the synthesized conjugated polymers to demonstrate that the simple introduction of π -conjugated units into the side chains could effectively improve the PCE of a PSC. The tailored polymer with the optimal side chains, PBDT2FBT-T3, exhibited the highest short-circuit current density (J_{sc}) among the polymers tested, 12.3 mA cm $^{-2}$, and a maximized PCE of 6.48%, without introducing any processing additives or post-treatments.

2. RESULTS AND DISCUSSION

2.1. Design, Synthesis and Characterization. The detailed synthetic procedures and characterization data of monomers are described in Scheme 1 and the Experimental Section. A weak electron-rich BDT unit was employed as the comonomer to construct D–A medium-bandgap copolymers bearing a strongly electron-deficient 5,6-difluorobenzothiadiazole (2FBT) unit through the “push-pull” interactions. The four different side chains (alkylated thienyl-, bithienyl-, terthienyl-, and quaterthienyl-) were attached to the central benzene ring of the BDT unit which has a flexibility of attaching different substituents. The large twisting motions of the thienyl plane relative to the BDT plane weakened the electron-donating properties of the 2D conjugated BDT-T unit by altering the backbone coplanarity in comparison with the BDT unit prepared with alkoxy side chains for use in photovoltaic polymers, thus providing a lower HOMO level.²⁹ Because maximum value of the V_{oc} is determined by the energy difference between the HOMO level of the donor and LUMO level of the acceptor, a deep HOMO level of donor polymer is desirable to yield a high V_{oc} .³⁰ Moreover, the use of fluorine atoms in the acceptor unit of a D–A copolymer has been shown to decrease the HOMO level. The smaller size of the fluorine atom as compared to other electron withdrawing

Table 2. Optical Properties and Molecular Energy Levels of PBDT2FBT-T_n

polymer	λ_{max} soln. (nm) ^a	λ_{max} film (nm) ^b	λ_{onset} film (nm) ^b	A_{0-2}/A_{0-1}	HOMO/LUMO (eV)		$E_{\text{g}}^{\text{calc}}$ (eV)	E_{g}^{EC} (eV)	$E_{\text{g}}^{\text{opt}}$ (eV) ^c
					DFT	cyclic voltammetry			
PBDT2FBT-T1	343, 407, 548	370, 442, 592	706	0.66	-5.02/-2.73	-5.47/-3.58	2.29	1.89	1.75
PBDT2FBT-T2	317, 391, 587	406, 604	717	0.67	-4.94/-2.76	-5.37/-3.61	2.18	1.76	1.73
PBDT2FBT-T3	410, 608	418, 613	726	0.94	-4.87/-2.77	-5.31/-3.62	2.10	1.69	1.70
PBDT2FBT-T4	425, 608	440, 618	737	1.63	-4.84/-2.76	-5.30/-3.63	2.08	1.67	1.68

^aMeasured in dilute chlorobenzene solution at a concentration of 0.05 g L⁻¹. ^bSpin-cast from 10 mg mL⁻¹ chlorobenzene solution. ^cEstimated from the onset of the UV-vis spectra measured from thin films.

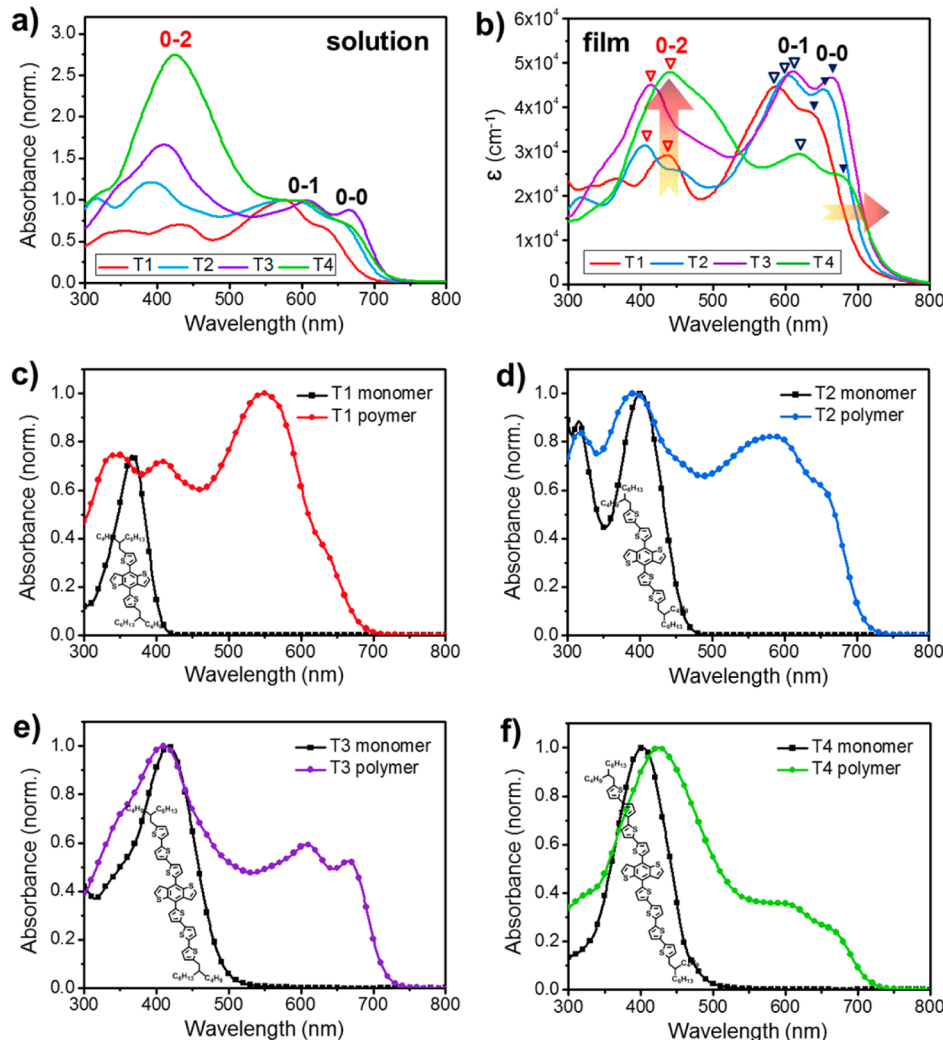


Figure 3. (a) Normalized UV-vis absorption spectra of PBDT2FBT-T_n polymers in DCB at a concentration of 0.125 mg mL⁻¹ at 25 °C. (b) UV-vis absorption coefficient of the PBDT2FBT-T_n polymers in spun cast films prepared by DCB. The reversed triangles indicate absorption band of A₀₋₀ (navy), A₀₋₁ (opened navy), and A₀₋₂ (opened red). For all polymers, we selected the maximum intensity in the low-wavelength region (300–550 nm) as A₀₋₂ for simple comparison even there exist another faint peaks. Absorption spectra of PBDT2FBT-T_n polymers and BDT-T_n monomers in DCB solution: (c) T₁, (d) T₂, (e) T₃, and (f) T₄.

groups did not introduce much steric hindrance into the polymer backbone. The synergistic effects of BDT and the fluorine substituent contributed to the potential utility of PBDT2FBT-based copolymer systems for use in BHJ-PSCs.³¹

The general procedure used to synthesize the four polymers is shown in Figure 2a. The target polymers were prepared through a Stille cross-coupling reaction between bis(trimethyltin) BDT and the dibrominated DT2FBT under nearly the same conditions. All reactions gave a yield of 60–

80%. The crude products were isolated using chloroform after Soxhlet extraction with methanol, acetone, and *n*-hexane. All four resulting copolymers exhibit good solubility in common solvents such as chloroform (CF), chlorobenzene (CB), and 1,2-dichlorobenzene (DCB), but their solubilities varied considerably at room temperature (Table 1). The number-average molecular weights (M_n) of the resulting polymers were 28.1, 42.8, 48.2, and 33.8 kDa, with polydispersity index (PDI) of 1.75, 1.13, 2.11, and 3.40, respectively.

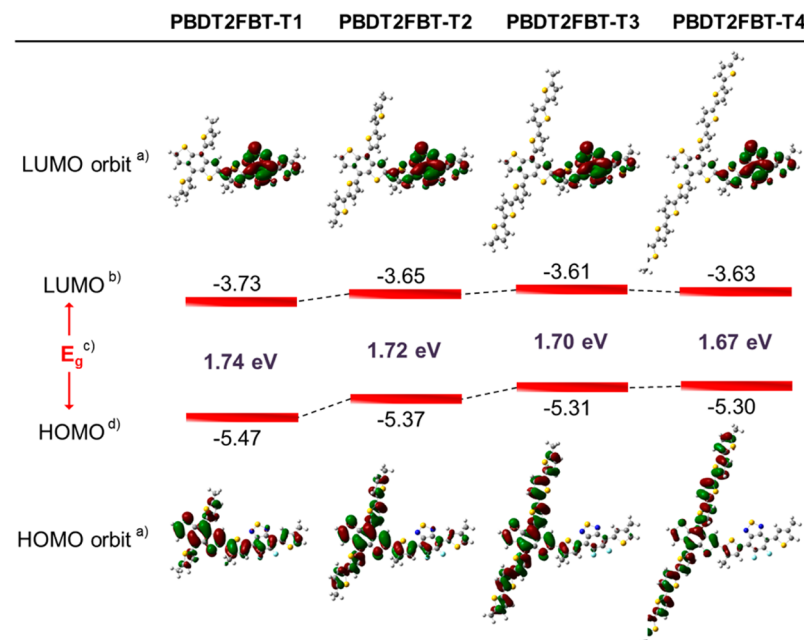


Figure 4. (a) Molecular orbital distribution of HOMO and LUMO for energy-minimized structure (B3LYP/6-31G*) of the model compounds at the bottom and top, respectively. The yellow, sky, and blue symbols represent sulfur, fluorine, and nitrogen atoms, respectively. (b) The LUMO energy levels are estimated by adding (c) the absorption onset to (d) the HOMO energy levels measured by cyclic voltammograms in thin films.

2.2. Thermal and Electrochemical Properties. Thermogravimetric analysis (TGA) was carried out to evaluate the thermal stabilities of the polymers under a nitrogen atmosphere. The four polymers with thienyl-, bithienyl-, terthienyl-, and quaterthienyl side chains displayed a decomposition temperature (defined as the 5% weight loss temperature, T_d) of 409, 422, 432, and 414 °C, respectively (Figure 2b). Since our results showed no significant differences between the T_d values of the four polymers, we concluded that the size and topology of the oligothienyl side chains attached to the BDT moiety did not play a critical role in determining the polymer thermal stability.

The actual HOMO and LUMO energy levels of the polymers were measured from the cyclic voltammograms as the onset potentials of the first oxidation and the reduction peaks, respectively, as shown in Figure 2c and summarized in Table 2. PBDT2FBT-T1 exhibited a deep-lying HOMO level of -5.47 eV, suggesting that the polymer would be stable against oxidization, leading to a high device stability; however, the HOMO levels of these four polymers gradually increased as the number of thienyl units increased in their side chains because the extended conjugation length reduced the bandgap of the 2D conjugated polymers. The LUMO energy levels of the polymers were estimated from the HOMO energy levels and the optical band gaps in the solid state according to the following equation: $E_{\text{LUMO}} = E_g^{\text{opt}} + E_{\text{HOMO}}$.³²

2.3. Optical Properties. UV-vis absorption spectra of PBDT2FBT-T_n in dilute chlorobenzene (CB) solutions and spin-coated films are shown in Figure 3, parts a and b, respectively. The detailed absorption data, including the absorption maxima and band edges in solution and film, are summarized in Table 2. The absorption spectra of these copolymers were characterized by two spectral features, a high-energy band attributed to the localized $\pi-\pi^*$ transition (A_{0-2}) and a lower-energy band ascribed to the intracharge transfer (ICT) transition (A_{0-1}) similar to other copolymers comprising D-A units.^{33,34}

In diluted CB solution, the optical properties may be regarded as the properties of single chain species undergoing rotation in a solvent with minimal intermolecular $\pi-\pi$ interactions because the polymer chains are isolated by the solvent molecules.²⁴ As shown in parts c-f of Figure 3, the high-energy bands of the PBDT2FBT-T_n polymers corresponded with those of the BDT-T_n monomers, suggesting that the differences in the high-energy absorptions of PBDT2FBT-T_n resulted from the π -conjugation along the oligothienyl side chains. In addition, the intensities of these absorption bands (the evolution of the A_{0-2}/A_{0-1} ratio) gradually increased as the number of thienyl units present in the side chains increased. This result clearly indicates that the light-harvesting properties of the parent conjugated polymers could be improved by introducing chromophoric side chains to broaden its absorption range and maximize overlap with the solar emission spectrum. In particular, low absorption of one-dimensional D-A conjugated polymer systems in the UV region, which appears in the shape of a biased dual band, can be improved using a 2D conjugation molecular design strategy.

The low-energy absorption band of conjugated polymers in the visible region is assigned mainly to the ICT transition characteristic of the conjugated main chain. As shown in Figure 3b, these 2D conjugated polymers displayed a gradual red-shift in the absorption band maxima (λ_{max}) and band edges in polymer thin films as the number of thienyl units increased in the side chains, for a given conjugated backbone. These red-shifts indicated that π -conjugation length of conjugated polymers could be extended by introducing 2D conjugated system.

All spectra obtained from these four polymers displayed a pronounced absorption shoulders (vibronic peaks) due to a strong interchain $\pi-\pi^*$ transition (A_{0-0}), indicating that the polymers strongly tended toward a structurally organized and orderly packed structure in the thin film state.^{35,36} The intensity of the vibronic peak (the evolution of the A_{0-0}/A_{0-1} ratio) gradually increased from PBDT2FBT-T1 to PBDT2FBT-T3.

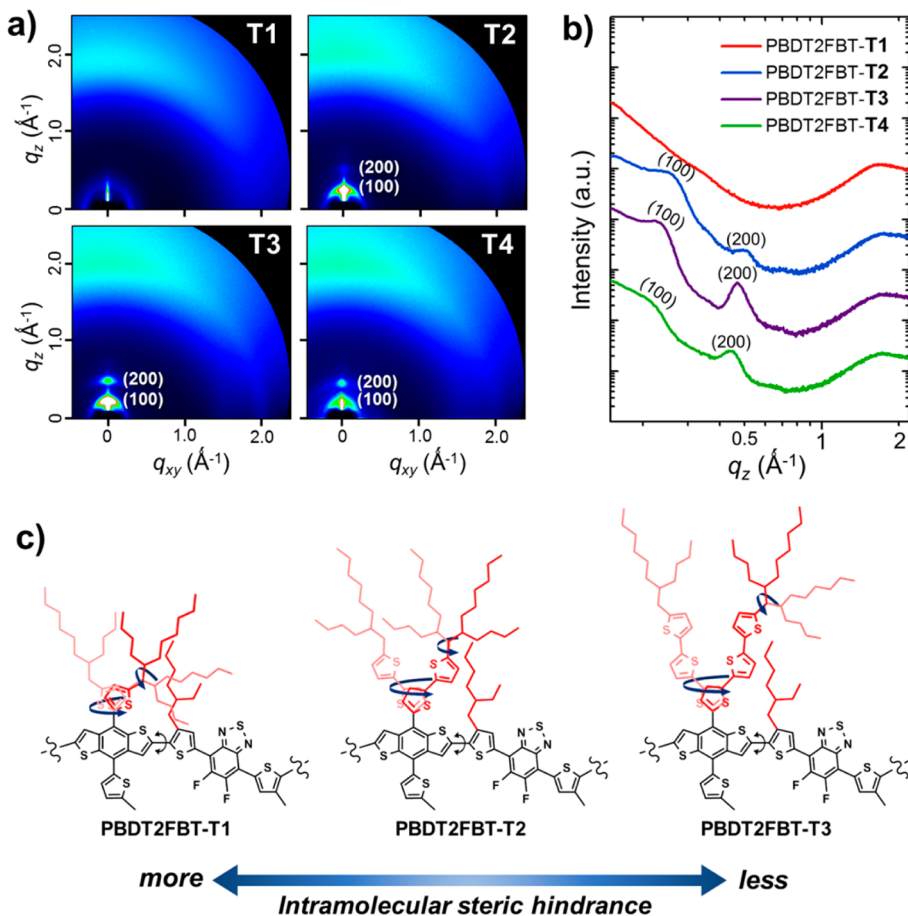


Figure 5. (a) 2D GIXD images and (b) 1D patterns of out-of-plane direction for neat polymer thin films. (c) Schematic illustration of intramolecular steric hindrance for PBDT2FBT-T_n polymers.

For PBDT2FBT-T4, however, the abrupt decrease in the vibronic peak intensity may have arisen from the oversized conjugated side chains, which reduced the coplanarity of the backbone, thereby decreasing the intermolecular chain packing of the polymer system.²⁸

2.4. Theoretical Calculations. Density functional theory (DFT) calculations using the B3LYP/6-31G* model^{37–40} were performed on single repeat units (BDT2FBT-T1, BDT2FBT-T2, BDT2FBT-T3, and BDT2FBT-T4) of the four polymers, using methyl-trimmed alkyl chains for simplicity, to explore the electronic and conformational structures of the polymers in depth (Figure 4). The theoretically predicted energy levels and energy gaps of the model structures are summarized in Table 2.

We plotted the frontier orbitals of the HOMO and LUMO of the single repeat units to elucidate the changes in the optical and electrochemical properties of the polymers given different side chain architectures. Our calculations indicated that the LUMOs of these four model compounds were essentially localized on a single fragment and displayed similar antibonding characteristics at the bridging atoms of each conjugated segment. By contrast, the HOMOs were distributed along the 2D conjugated system, including the oligothienyl side chains, suggesting that the π-electrons were delocalized further upon introducing the 2D conjugated system. Interestingly, the HOMOs are less and less delocalized along the main backbone even further delocalized on the 2D conjugated system with the increase of the thienyl unit. The overlap between the HOMO and the LUMO on the 2FBT unit is also decreasing. This could

explain why the ICT absorption band is decreasing significantly for PBDT2FBT-T4 (Figure 3).

The values of HOMO energy levels of the model compounds were observed to increase with the number of thienyl units present (Table 2). Extending the π-conjugation length along the side chains decreased the bandgap of the polymer systems, thereby improving the absorption properties, in accordance with the results obtained using UV-vis spectroscopy (Figure 3).

2.5. Crystalline Structures of Neat Polymer Films. Grazing incident X-ray diffraction (GIXD) patterns were measured to understand the molecular packing and the crystalline structures of the polymers in the neat films. Note that a diffraction peak of PBDT2FBT-T1 was very weak in the neat polymer films (Figure 5, parts a and b), implying an amorphous polymeric property. The bulky and branched alkyl side chain (2-butyloctyl) appended to the monothienyl unit (T1) on the BDT unit has a strong chance to induce an intramolecular steric hindrance with adjacent alkyl side chain (2-ethylhexyl) on the π-conjugated bridge thienyl unit (Figure 5c). However, the intramolecular steric hindrance in this series of 2D conjugated system could be decreased as the number of thienyl units increased because the numerically extended thienyl units put some distance between the bulky 2-butyloctyl and 2-ethylhexyl alkyl chains. The topological aspects of side chains in this 2D conjugated system led to significant differences in the molecular packing and crystalline property in the thin films. PBDT2FBT-T3 showed most distinct

diffraction patterns, implying a higher crystalline property. For PBDT2FBT-T4, however, an abrupt decrease of crystalline property was observed probably due to the oversized conjugated side chains to induce a large intermolecular steric hindrance with neighboring polymers in the films, which is accordance with a decreased intensity of the ICT absorption band.

The interchain d_{lamellar} spacings of PBDT2FBT-T2, -T3, and -T4 were 24.6, 27.7, and 30.2 Å, respectively. Note that the much smaller d_{lamellar} spacings in the PBDT2FBT-T n polymer chains, as observed in the GIXD results, compared to the 2-fold intrinsic lengths of the side chains calculated based on the DFT results suggested that interdigitated packing structures were constructed between the stacked lamella, as illustrated in Figure 6. It is presumed that the presence of repetitive oligothienyl units along the side chains permitted the formation of an interdigitated packing structure. This interdigitated lamellar packing structure extended the linearity of the backbone, facilitated the formation of π -stacking structures between the polymer backbones, and promoted the formation of highly

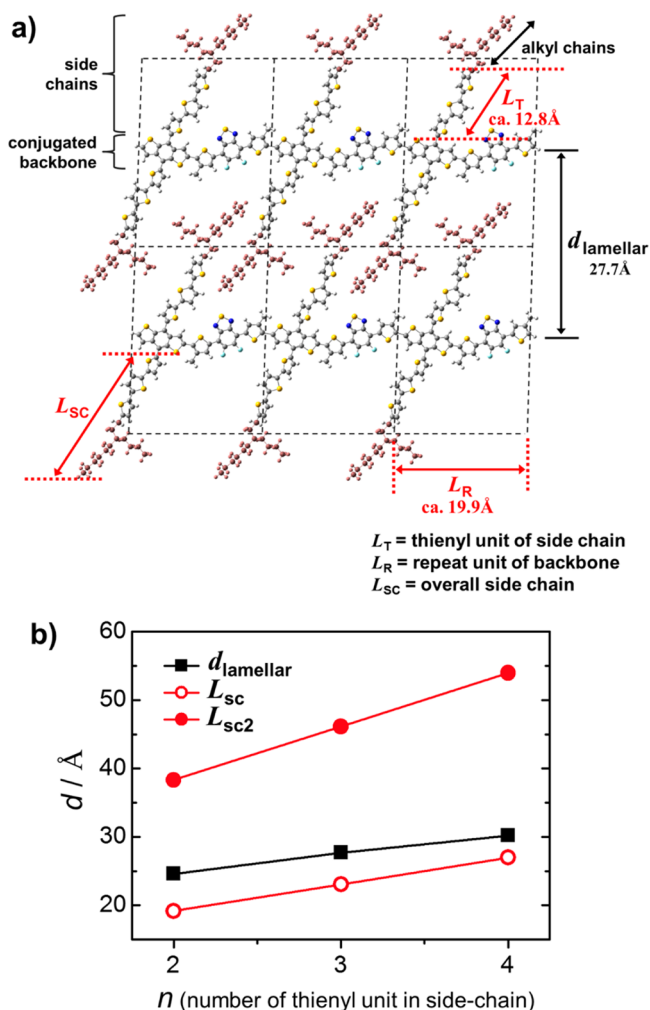


Figure 6. (a) Schematic diagram of two-dimensionally stacked packing structure of PBDT2FBT-T3 polymer molecule with side chain interdigitation. 2-Ethylhexyl alkyl chains on the backbone were trimmed for simplicity. (b) Plots of the d_{lamellar} and $d_{\text{side-chain}}$ value vs the number of thietyl unit in the side chain. d_{lamellar} , L_{sc} and $L_{\text{sc}2}$ are lamellar d -spacing, length of side chain, and 2-fold length of side chain, respectively.

ordered laterally extended microstructures composed of π -stacked lamella.⁴¹

2.6. Photovoltaic Performance. BHJ-PSC devices with the configuration ITO/MoO₃/polymer:PC₇₁BM/LiF/Al were fabricated to investigate and compare the photovoltaic properties of these four 2D conjugated polymers. The devices were fabricated using PBDT2FBT-T n as donor materials and PC₇₁BM as an acceptor material. The solvent DCB was chosen for processing because it readily dissolves PBDT2FBT-T n and has a high boiling point, which is advantageous for developing nanoscale morphologies in the photoactive layers.^{42–44} The solubilities of the four polymers are listed in Table 1. We fabricated photovoltaic devices using various donor and acceptor weight ratios (1:0.7, 1:0.8, 1:0.9, 1:1, 1:1.2, 1:1.5, and 1:2) and a wide range of photoactive layer thicknesses to optimize the PCEs (Tables S1 and S2, Supporting Information). The photovoltaic performances depended significantly on the thietyl side chains of the polymers and the PBDT2FBT-T3:PC₇₁BM-based PSCs reached a maximum PCE of 6.48%, with a V_{oc} of 0.86 V, J_{sc} of 12.3 mA cm⁻², and fill factor (FF) of 61.4%. The trends in the photovoltaic parameters for the optimal PCE results of four polymer-based OPV device will be discussed below.

The V_{oc} values of each optimized device decreased gradually from 0.98 to 0.84 V as the number of thietyl units in the side chains increased because the HOMO levels increased monotonically, as confirmed by the CV and DFT results. V_{oc} is mainly determined by the difference between the HOMO level of the donor polymer and the LUMO level of the PC₇₁BM;³⁰ therefore, the increase of the HOMO levels in this 2D conjugated system, from -5.47 to -5.30 eV, largely accounted for the decrease in V_{oc} . Although the anisotropic π -conjugation expansion of this 2D conjugated system increased the HOMO level, the solar cell based on PBDT2FBT-T4, which showed the highest HOMO level of -5.30 eV in this series of polymers, still exhibited a high V_{oc} value of 0.84 V. The synergic effects between the fluorine atoms, which acted as strong electron-withdrawing substituents, and the BDT units, which acted as weak donors, produced deep-lying HOMO levels in the PBDT2FBT-T n series.

Unlike the trends in V_{oc} , the J_{sc} values increased from 9.62 to 12.3 mA cm⁻² with the increase of the thietyl unit from T1 to T3, as confirmed by the external quantum efficiencies (η_{EQE}) and estimated J_{sc} values obtained from the η_{EQE} results (Figure 7b and Table 3); however, the J_{sc} of PBDT2FBT-T4 was reduced abruptly to 6.35 mA cm⁻². The difference between the η_{EQE} values of polymers mainly resulted from the light absorption efficiency (η_A) and the internal quantum efficiency (η_{IQE}) with the sequential steps involved in exciton diffusion (η_{ED}), exciton dissociation through charge transfer (η_{CT}), and the collection of free charge carriers as a result of charge transport (η_{CC}) in the corresponding devices: $\eta_{\text{EQE}} = \eta_A \eta_{\text{IQE}} = \eta_A \eta_{\text{ED}} \eta_{\text{CT}} \eta_{\text{CC}}$.^{45,46} The PSC device performances were analyzed by evaluating η_A , η_{IQE} , and η_{EQE} (Figure 7b and Figure 8).^{45–50}

The values of η_A for the photovoltaic devices prepared using the PBDT2FBT-T n :PC₇₁BM blend films featured a distinct increase in both the short wavelength and long wavelength regions with the increase of the thietyl unit up to T3. This trend resulted from the enhanced absorption of the $\pi-\pi^*$ transition (blue absorption band) and the ICT transition (red absorption band) (Figure 8a). The PC₇₁BM also contributed to the overall absorption of the blend film in the short wavelength region because the corresponding films were based on the

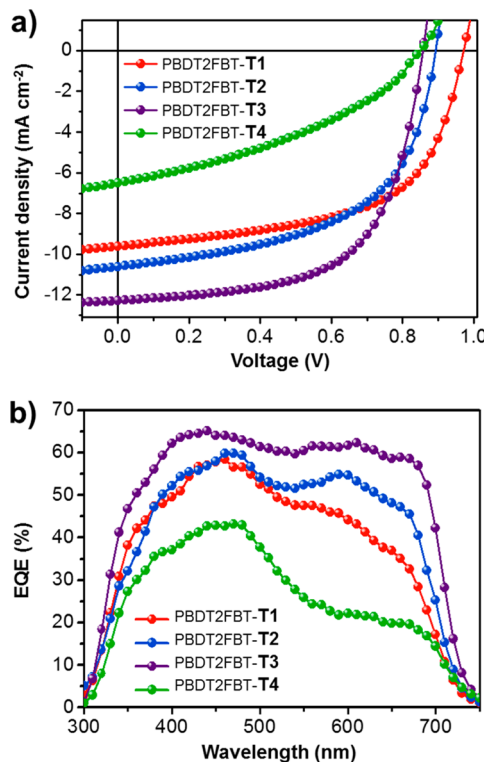


Figure 7. (a) J – V characteristics of PBDT2FBT- Tn :PC₇₁BM solar cell prepared by DCB measured under illumination of AM 1.5G, 100 mW cm⁻² and (b) EQE curves of the corresponding polymer solar cells.

mixture of conjugated polymers and fullerene.⁵¹ The values of η_A were evaluated by recording the reflectance spectra of the devices (R_d) and the electrodes (R_e) (see Figure S21 in the Supporting Information): $\eta_A = 100(1 - R_d/R_e)$.^{49,50} The photoactive layer based on PBDT2FBT-T3 displayed the most extended absorption behaviors among the four polymer-based blend films tested here and the enhanced light absorption positively contributed to photocurrent generation.

The η_{IQE} values were enhanced over a more extensive range in the PBDT2FBT-T2 and PBDT2FBT-T3 devices compared with the values obtained from the other two devices. These η_{IQE} values reached 96.7% (PBDT2FBT-T2) and 99.8% (PBDT2FBT-T3) at 480 nm (Figure 8b). The η_{IQE} depends on an exciton dissociation by charge transfer followed by charge transport to the electrodes. These processes were evaluated by measuring the photoluminescence (PL) quenching efficiency (Figure S22) and the charge carrier mobility (Figure S23 and Figure S24), respectively. The PL quenching efficiencies of the PBDT2FBT- Tn :PC₇₁BM blend films were found to exceed 96% in all photoactive layers, indicating that the excitons were well-dissociated into free charge carriers, regardless of the side

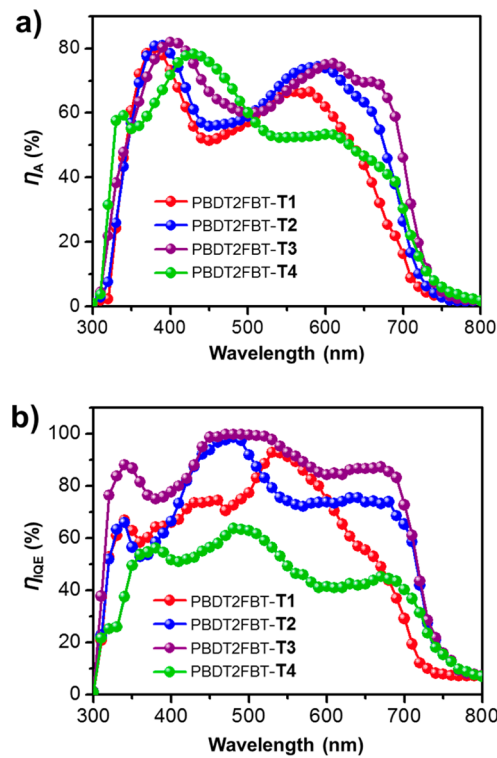


Figure 8. (a) Light absorption (η_A) and (b) internal quantum efficiencies (η_{IQE}) of the PBDT2FBT- Tn :PC₇₁BM based polymer solar cells.

chains.^{52,53} The enhanced η_{IQE} in the device based on PBDT2FBT-T3 appeared to be affected mainly by the transport of charge carriers.

The effects of the various oligothienyl side chains on charge carrier transport were explored by measuring the space-charge-limited-current (SCLC)^{54,55} and the field-effect transistor (FET) mobilities.⁵⁶ We fabricated SCLC devices with hole-only and electron-only structures, and FETs were prepared with bottom-gate and top-contact configurations. The dark current densities (J_D) in the SCLC devices with hole-only and electron-only structures were multiplied by the cube of the film thickness (L) to account for variations in the active layer thickness (Figure S23). The drain currents of the FETs with different gate biases are shown in Figure S24. The charge carrier mobilities varied with the difference in the side chain structures (Table S5). The hole and electron mobilities of the PBDT2FBT-T3 photoactive layer devices were 2.31×10^{-4} cm² V⁻¹ s⁻¹ and 2.04×10^{-3} cm² V⁻¹ s⁻¹, respectively, and the ratio of the electron mobility to the hole mobility reached 8.83. The estimated FET mobility of PBDT2FBT-T3 displayed a value as high as 2.48×10^{-4} cm² V⁻¹ s⁻¹. Both the SCLC and

Table 3. Photovoltaic Properties of PSCs Based on PBDT2FBT- Tn :PC₇₁BM

polymer	ratio ^a	thickness (nm) ^b	V_{oc} (V)	J_{sc} ($J_{sc,cal,c}$) (mA cm ⁻²)	FF (%)	PCE _{max} (PCE _{ave}) (%) ^d
PBDT2FBT-T1	1:1.2	91	0.98	9.62 (9.3)	59.7	5.46 (5.36)
PBDT2FBT-T2	1:0.8	118	0.90	10.6 (10.6)	54.7	5.22 (5.11)
PBDT2FBT-T3	1:0.8	140	0.86	12.3 (12.5)	61.4	6.48 (6.45)
PBDT2FBT-T4	1:1	95	0.84	6.35 (6.0)	40.5	2.17 (2.15)

^aPolymer:PC₇₁BM blend ratio (wt %). ^bThickness of active layer was measured by surface profiler (Alpha-step 500). ^cCalculated J_{sc} from the integrated area of the EQE spectrum. ^dPerformance metrics are average numbers from eight devices of each type under the illumination condition of AM 1.5G, 100 mW cm⁻². DCB was used as a processing solvent for all polymers.

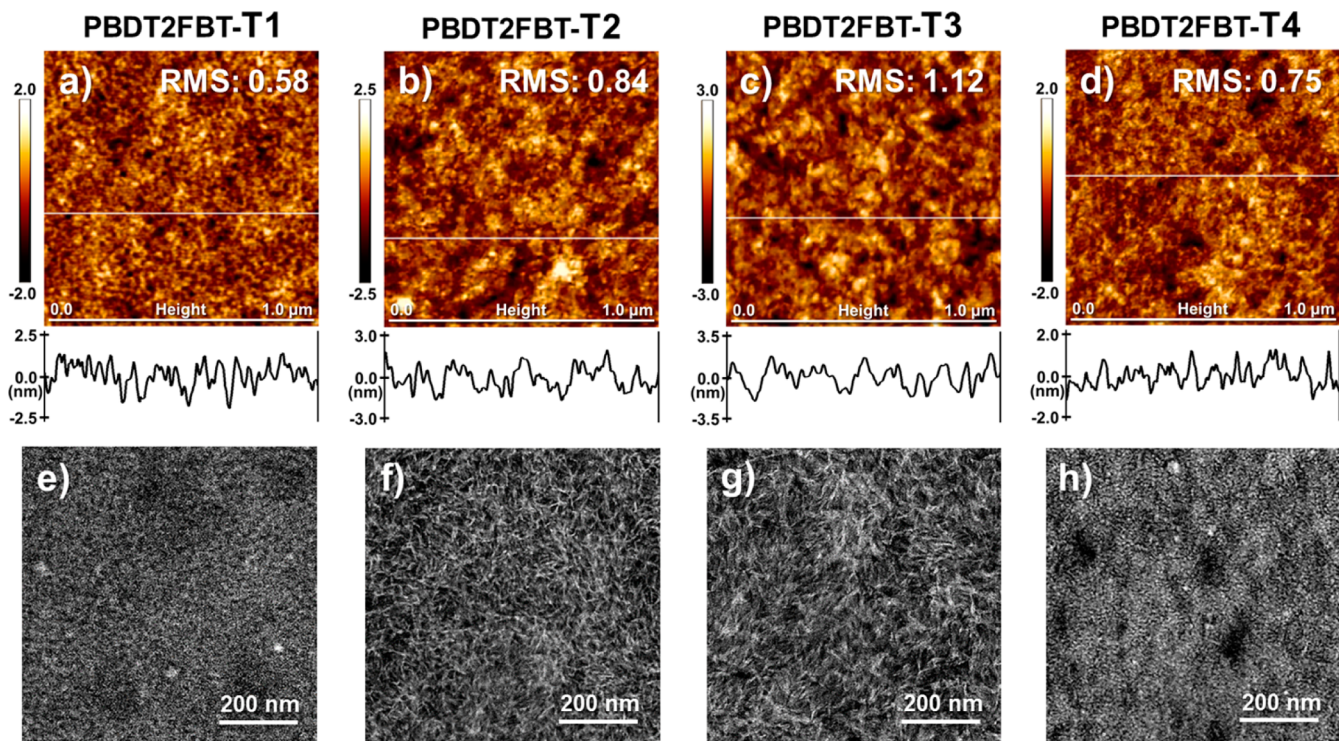


Figure 9. (a–d) AFM height images ($1.0\text{ }\mu\text{m} \times 1.0\text{ }\mu\text{m}$) and (e–h) TEM images of PBDT2FBT-T n :PC $_{71}$ BM blend films prepared by DCB.

FET devices based on PBDT2FBT-T3 showed higher mobility values compared to those of devices based on PBDT2FBT-T1, -T2, and -T4. The enhanced intermolecular chain packing and isotropically extended π -conjugation in PBDT2FBT-T3 appeared to promote carrier transport in the corresponding photoactive layers, resulting in a higher hole mobility. Bimolecular recombination between separated charges and space-limited charges may be significantly reduced in the PBDT2FBT-T3-based device. Therefore, the PBDT2FBT-T3-based device generated a more photocurrent than the devices prepared using other polymers due to the high internal quantum efficiency based on the facilitated carrier transport and enhanced the absorption efficiency.

2.7. Morphology of Photoactive Layers. The nanoscale morphologies of the PBDT2FBT-T n :PC $_{71}$ BM blend films were visualized using tapping-mode atomic force microscopy (TM-AFM) (Figure 9a–d) and transmission electron microscopy (TEM) (Figure 9e–h). The PBDT2FBT-T3:PC $_{71}$ BM blend films showed a most rough surface, with an RMS roughness of 1.12 nm. The enhanced crystalline property of polymers induced the increase in the surface roughness from T1 to T3 by promoting the formation of aggregated domains. The TEM images also revealed the presence of the enhanced fibrillar morphology in a similar aspect with the AFM result. The formation of polymer fibrillar structures could provide percolation pathways for the efficient charge carrier transports in the PBDT2FBT-T3:PC $_{71}$ BM-based photoactive layers.^{56–59}

The molecular orientation, intermolecular distance, and crystallinity in the blend films based on PBDT2FBT-T n polymers were investigated by measuring the GIXD patterns (Figure 10). The two-dimensional GIXD patterns of the polymer thin films showed pronounced diffraction peaks in the out-of-plane direction except for PBDT2FBT-T1, indicating that edge-on crystal orientations were preferred in the blend films.^{60,61} The blend films prepared using PBDT2FBT-T2,

PBDT2FBT-T3, or PBDT2FBT-T4 displayed (100) lamellar stacking peaks along the out-of-plane direction at q -values of 0.255, 0.227, and 0.208 \AA^{-1} , respectively, which corresponded to the d -spacing values of 24.6, 27.7, and 30.2 \AA , respectively. The PBDT2FBT-T1 blend film did not display distinct crystal peaks like as the neat films. Long-range packing order is quantitatively measured by determining correlation length (L_C) of the polymers in the optimized active layers using the Scherrer eq ($2\pi K/\text{fwhm}$), which is defined as the length over which a crystalline structure is preserved.⁶² The coherence lengths of the blend films prepared using PBDT2FBT-T2, PBDT2FBT-T3, and PBDT2FBT-T4 were calculated to be 9.8, 12.7, and 8.8 nm, respectively. The higher degree of crystalline ordering for the PBDT2FBT-T3:PC $_{71}$ BM films demonstrated convincingly that optimal extension of π -conjugated side chains in the 2D conjugated system can effectively enhance the crystalline property of parent polymer.

3. CONCLUSIONS

In summary, a 2D conjugation system composed of D–A medium-bandgap polymers was prepared via a side chain engineering approach with the aim of improving the PCEs of PSCs prepared using these polymers. The optimum size of the chromophoric side chains in the conjugated polymers was crucial for balancing light absorption and carrier transport. PBDT2FBT-T3 showed the highest PCE, 6.5%, among the conjugated polymers tested, with an extended absorption spectrum and high carrier transport. Our study provides new insights into the molecular design and synthesis of highly efficient PSCs.

4. EXPERIMENTAL SECTION

4.1. Characterization. All monomers were characterized by ^1H NMR (400 MHz) and ^{13}C NMR (100 MHz) on a Bruker AVANCE 400 spectrometer in chloroform-d solutions at room temperature. All

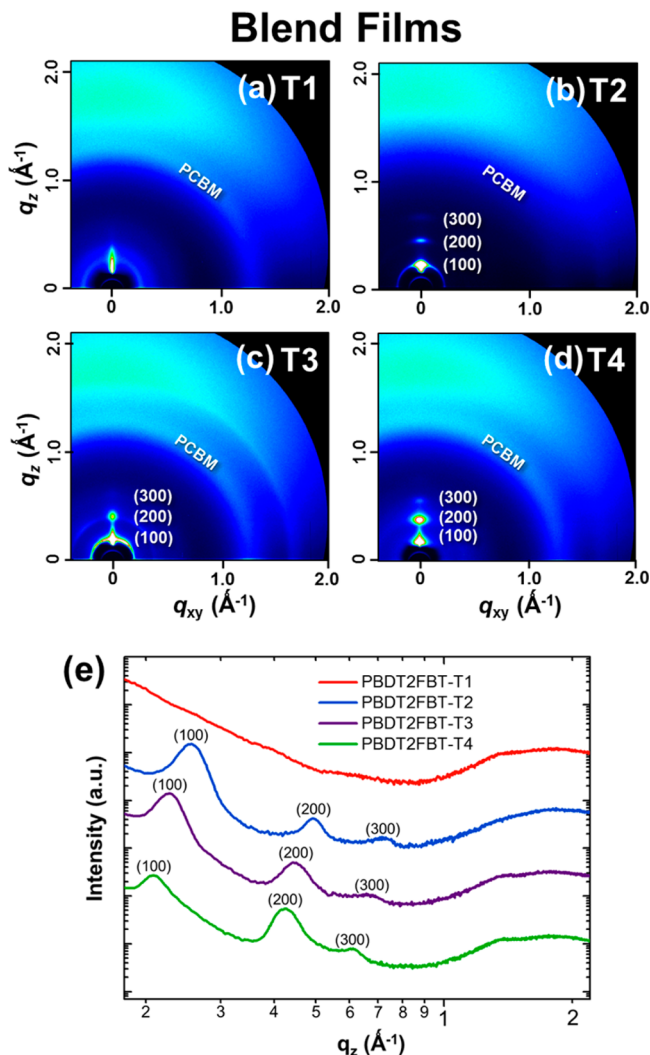


Figure 10. (a) 2D GIXD images and (b) 1D patterns of out-of-plane direction for PBDT2FBT-T_n:PC₇₁BM blend films prepared by DCB.

polymers were characterized by ¹H NMR (500 MHz) on Bruker DRX 500 spectrometer in 1,2-dichlorobenzene-*d*₄ at 383 K due to low solubility of PBDT2FBT-T2 and -T3. Number-average (M_n) and weight-average (M_w) molecular weights were determined with gel permeation chromatography (GPC, Shimadzu) in chlorobenzene at 80 °C, using two PL mixed B columns in series, and calibrated against narrow polydispersity polystyrene standards. UV-vis spectra were recorded on a Varian CARY-5000 UV-vis spectrophotometer. For the measurements of thin films, polymers were spun coated onto precleaned glass substrates from chlorobenzene solutions (10 mg mL⁻¹). TGA plots were measured with a TA Instruments, Inc., TGA 2050 under a nitrogen atmosphere at heating and cooling rates of 10 °C·min⁻¹. AFM and TEM images were obtained with a MultiMode 8 Scanning Probe Microscope (VEECO Instruments Inc.) and a Hitachi-7600 system by using an accelerating voltage of 100 kV, respectively. GIXD measurements were performed using the 3C and 9A (2D) beamlines at the Pohang Accelerator Laboratory (PAL).

4.2. Synthesis of Monomers. 2-(2-Butyloctyl)thiophene (1). To a solution of thiophene (5.0 g, 59.4 mmol) in THF (10 mL) in an N₂ purged flask was added *n*-BuLi (1.6 M in THF, 40.8 mL, 1.1 equiv) dropwise at -78 °C. The solution was stirred for 90 min at 55 °C before 2-butyloctyl bromide (14.3 g, 57.6 mmol) was dropwise added. After 120 min, the reaction mixture was cooled to room temperature, and then aqueous NaCl solution (2.0 M in 20 mL) was added. The solution was stirred for another 60 min before it was poured into water and extracted with CH₂Cl₂ (100 mL × 3). The combined extracts

were dried with anhydrous MgSO₄ and evaporated. The crude product was purified by vacuum distillation to give pure **1** as a pale yellow oil (10.8 g, yield 72%). ¹H NMR (CDCl₃, 400 MHz), δ (ppm): 7.10 (d, 1H), 6.92 (t, 1H), 6.75 (d, 1H), 2.75 (d, 2H), 1.61 (m, 1H), 1.4–1.15 (m, 16H), 0.94–0.80 (m, 6H). MALDI-MS: calcd, *m/z* = 252.5; found, 252.4 [M⁺].

5-(2-Butyloctyl)-2,2'-bithiophene (3). 2-(2-Butyloctyl)thiophene-5-bromide (5.0 g, 15.0 mmol), 2-(trimethylstannyl)thiophene (3.7 g, 15.0 mmol), and tetrakis(triphenylphosphine)palladium(0) (350 mg, 2.0 mol %) were added to a three neck flask under a nitrogen atmosphere followed by the addition of toluene (50 mL) and DMF (5 mL). The reaction mixture was stirred at 105 °C for 48 h and then cooled to room temperature. The crude product was extracted with CH₂Cl₂ (100 mL × 3) and purified by column chromatography with *n*-hexane:dichloromethane = 10:1 (v:v) as eluent. The solvent was evaporated and the product was recrystallized from 2-propanol as pale orange solid (3.18 g, yield 63%). ¹H NMR (CDCl₃, 400 MHz), δ (ppm): 7.15 (d, 1H), 7.10 (d, 1H), 7.00 (d, 1H), 6.98 (t, 1H), 6.65 (d, 1H), 2.07 (d, 2H), 1.62 (m, 1H), 1.33–1.18 (m, 16H), 0.94–0.80 (m, 6H). MALDI-MS: calcd, *m/z* = 334.2; found, 334.2 [M⁺].

5-(2-Butyloctyl)-2,2';5',2"-terthiophene (5). 2-(2-Butyloctyl)-thiophene-5-bromide (4.0 g, 12.0 mmol), 5-(trimethylstannyl)-2,2'-bithiophene (3.98 g, 12.0 mmol), and tetrakis(triphenylphosphine)-palladium(0) (280 mg, 2.0 mol %) were added to a three neck flask under a nitrogen atmosphere followed by the addition of toluene (50 mL) and DMF (5 mL). The reaction mixture was stirred at 105 °C for 48 h and then cooled to room temperature. The crude product was extracted with CH₂Cl₂ (100 mL × 3) and purified by column chromatography with *n*-hexane:dichloromethane = 8:2 (v:v) as eluent. The solvent was evaporated and the product was recrystallized from 2-propanol as orange solid (3.37 g, yield 67%). ¹H NMR (CDCl₃, 400 MHz), δ (ppm): 7.19 (d, 1H), 7.15 (d, 1H), 7.06 (d, 1H), 7.02 (d, 1H), 7.00 (d, 1H), 6.98 (t, 1H), 6.66 (d, 1H), 2.72 (d, 2H), 1.63 (m, 1H), 1.36–1.13 (m, 16H), 0.94–0.83 (m, 6H). MALDI-MS: calcd, *m/z* = 416.2; found, 416.8 [M⁺].

5-(2-Butyloctyl)-2,2';5',2";5",2"-quaterthiophene (7). 2-(2-Butyloctyl)thiophene (3.0 g, 9.1 mmol), 5-(trimethylstannyl)-2,2';5',2"-terthiophene (3.72 g, 9.1 mol), and tetrakis(triphenylphosphine)palladium(0) (210 mg, 2.0 mol %) were added to a three neck flask under a nitrogen atmosphere followed by the addition of toluene (50 mL) and DMF (5 mL). The reaction mixture was stirred at 105 °C for 48 h and then cooled to room temperature. The crude product was extracted with CH₂Cl₂ (100 mL × 3) and purified by column chromatography with *n*-hexane:dichloromethane = 7:3 (v:v) as eluent. The solvent was evaporated and the product was recrystallized from 2-propanol as pale orange solid (3.20 g, yield 71%). ¹H NMR (CDCl₃, 400 MHz), δ (ppm): 7.24 (d, 1H), 7.21 (d, 1H), 7.08 (d, 1H), 7.06 (d, 1H), 7.01 (d, 1H), 7.00 (d, 1H), 7.01 (d, 1H), 6.99 (t, 1H), 6.66 (d, 1H), 2.72 (d, 2H), 1.63 (m, 1H), 1.38–1.18 (m, 16H), 0.92–0.83 (m, 6H). MALDI-MS: calcd, *m/z* = 498.2; found, 498.2 [M⁺].

General Synthetic Procedure of BDT-T_n Monomers. Substitution of Thietyl Side Groups (8). Under nitrogen atmosphere, *n*-BuLi (1.6 M in THF, 1.1 equiv) was added dropwise to a solution of **T1** (or **T2**, **T3**, **T4**) in dry THF at 0 °C. The mixture was then warmed to 50 °C and stirred for 1 h. Subsequently, 4,8-dihydrobenzo[1,2-*b*;4,5-*b'*]dithiophen-4,8-dione was added to the reaction mixture, which was then stirred for another 1 h at 50 °C. Cooling the mixture down to ambient temperature, SnCl₂·2H₂O (4.5 g, 20 mmol) in 8 mL HCl (10%) was added, and the mixture was stirred for another 4 h. The mixture was subsequently poured into ice water and extracted with CH₂Cl₂ (100 mL × 3). The combined extracts were dried with anhydrous MgSO₄ and evaporated. The crude product was purified by column chromatography on silica gel to give pure BDT-T_n.

4,8-Bis(5-(2-butyloctyl)thiophene-2-yl)benzo[1,2-*b*;4,5-*b'*]dithiophene. The crude product was purified by column chromatography on silica gel eluting with dichloromethane:hexane = 1:10 (v:v) to give pure product as a pale yellow liquid. (yield 61%). ¹H NMR (CDCl₃, 400 MHz), δ (ppm): 7.64 (d, 2H), 7.45 (d, 2H), 7.29 (d, 2H), 6.88 (d, 2H), 2.85 (d, 4H), 1.72 (m, 2H), 1.48–1.25 (br, 32H),

0.94–0.88 (m, 12H). $^{13}\text{CNMR}$ (CDCl_3 , 100 MHz), δ (ppm): 145.86, 139.14, 137.34, 136.65, 127.8, 127.58, 125.53, 124.31, 123.56, 40.16, 34.82, 33.51, 33.18, 31.95, 29.62, 29.05, 26.78, 23.21, 23.18, 22.85, 14.31. MALDI–MS: calcd, m/z = 690.3; found, 691.2 [M^+].

4,8-Bis(5'-(2-butyloctyl)-[2,2'-bithiophen]-5-yl)benzo[1,2-b:4,5-b']dithiophene. The crude product was purified by column chromatography on silica gel eluting with dichloromethane:hexane = 1:10 (v:v) to give pure product as a yellow solid. (yield 64%). $^1\text{H NMR}$ (CDCl_3 , 400 MHz), δ (ppm): 7.69 (d, 2H), 7.46 (d, 2H), 7.39 (d, 2H), 7.24 (d, 2H), 7.09 (d, 2H), 6.70 (d, 2H), 2.77 (d, 4H), 1.66 (m, 2H), 1.38–1.20 (br, 32H), 0.95–0.86 (m, 12H). $^{13}\text{CNMR}$ (CDCl_3 , 100 MHz), δ (ppm): 144.79, 139.19, 138.43, 137.85, 137.19, 137.18, 135.12, 128.97, 128.62, 126.41, 125.14, 124.37, 123.12, 40.15, 34.72, 33.34, 33.17, 31.98, 29.77, 28.99, 26.75, 25.37, 23.18, 22.83, 14.26. MALDI–MS: calcd, m/z = 854.3; found, 855.2 [M^+].

4,8-Bis(5'-(2-butyloctyl)-[2,2';5',2"-terthiophen]-5-yl)benzo[1,2-b:4,5-b']dithiophene. The crude product was purified by column chromatography on silica gel eluting with dichloromethane:hexane = 2:8 (v:v) to give pure product as a yellow ochre solid. (yield 61%). $^1\text{H NMR}$ (CDCl_3 , 400 MHz), δ (ppm): 7.71 (d, 2H), 7.52 (d, 2H), 7.41 (d, 2H), 7.29 (d, 2H), 7.16 (d, 2H), 7.05 (d, 2H), 7.03 (d, 2H), 6.69 (d, 2H), 2.76 (d, 4H), 1.65 (m, 2H), 1.38–1.20 (br, 32H), 0.95–0.86 (m, 12H). $^{13}\text{CNMR}$ (CDCl_3 , 100 MHz), δ (ppm): 144.53, 139.25, 138.54, 138.23, 137.89, 137.51, 136.74, 135.15, 134.78, 129.17, 128.09, 126.12, 124.75, 123.73, 123.60, 123.54, 123.41, 40.12, 34.74, 33.36, 33.25, 33.17, 32.04, 29.78, 29.02, 26.75, 23.16, 22.84, 14.30. MALDI–MS: calcd, m/z = 1018.3; found, 1019.3 [M^+].

4,8-Bis(5'-(2-butyloctyl)-[2,2';5',2"-quaterthiophene]-5-yl)benzo[1,2-b:4,5-b']dithiophene. The crude product was purified by column chromatography on silica gel eluting with dichloromethane:hexane = 3:7 (v:v) to give pure product as a dark yellow solid. (yield 68%). $^1\text{H NMR}$ (CDCl_3 , 400 MHz), δ (ppm): 7.72 (d, 2H), 7.53 (d, 2H), 7.43 (d, 2H), 7.35 (d, 2H), 7.18 (d, 2H), 7.11 (d, 2H), 7.09 (d, 2H), 7.03 (d, 2H), 7.00 (d, 2H), 6.68 (d, 2H), 2.75 (d, 4H), 1.64 (m, 2H), 1.38–1.20 (br, 32H), 0.94–0.85 (m, 12H). $^{13}\text{CNMR}$ (CDCl_3 , 100 MHz), δ (ppm): 144.47, 137.18, 136.21, 135.31, 135.26, 134.76, 134.53, 128.04, 126.09, 125.01, 124.98, 124.37, 124.17, 123.84, 123.67, 123.52, 123.24, 123.15, 122.93, 122.62, 122.54, 40.10, 34.73, 33.34, 33.16, 33.03, 32.04, 29.78, 29.00, 26.74, 23.15, 22.83, 14.26. MALDI–MS: calcd, m/z = 1182.3; found, 1183.2 [M^+].

Stannylation of 8. Compound 8 was dissolved in dry THF in a nitrogen purged flask. The solution was cooled to –78 °C before *n*-BuLi (1.6 M in THF, 2.3 equiv) was added dropwise. After the reaction was stirred at –78 °C for 90 min, trimethyltin chloride (1 M in hexane, 2.6 equiv) was added in one portion. The solution was allowed to warm to room temperature slowly and stirred overnight. After the reaction, the solution was diluted with dichloromethane (200 mL), washed with water (150 mL × 3), dried over anhydrous MgSO_4 , and evaporated. The crude product was purified by recrystallization in 2-propanol to give pure distannylated BDT-Tn.

2,6-Bis(trimethyltin)-4,8-bis(5-(2-butyloctyl)thiophene-2-yl)benzo[1,2-b:4,5-b']dithiophene (BDT-T1). A pale yellow viscous oil (yield 55%). $^1\text{H NMR}$ (CDCl_3 , 400 MHz), δ (ppm): 7.68 (s, 2H), 7.31 (d, 2H), 6.90 (d, 2H), 2.86 (d, 4H), 1.74 (m, 2H), 1.45–1.25 (br, 32H), 0.95–0.86 (m, 12H), 0.39 (s, 18H). $^{13}\text{CNMR}$ (CDCl_3 , 100 MHz), δ (ppm): 145.52, 143.45, 142.38, 138.14, 137.47, 131.30, 127.69, 125.45, 122.57, 40.19, 34.89, 33.64, 33.23, 31.97, 29.85, 29.10, 26.86, 25.43, 23.20, 22.84, 14.29, –8.22. Anal. Calcd for $\text{C}_{48}\text{H}_{74}\text{S}_4\text{Sn}_2$: C, 56.70; H, 7.34; S, 12.61. Found: C, 56.64; H, 7.33; S, 12.50. MALDI–MS: calcd, m/z = 1016.27; found, 1017.1 [M^+].

2,6-Bis(trimethyltin)-4,8-bis(5'-(2-butyloctyl)-[2,2'-bithiophen]-5-yl)benzo[1,2-b:4,5-b']dithiophene (BDT-T2). A yellow solid (yield 72%). $^1\text{H NMR}$ (CDCl_3 , 400 MHz), δ (ppm): 7.71 (s, 2H), 7.40 (d, 2H), 7.25 (d, 2H), 7.10 (d, 2H), 6.71 (d, 2H), 2.77 (d, 4H), 1.66 (m, 2H), 1.38–1.22 (br, 32H), 0.95–0.86 (m, 12H), 0.41 (s, 18H). $^{13}\text{CNMR}$ (CDCl_3 , 100 MHz), δ (ppm): 144.45, 143.61, 143.09, 138.93, 138.65, 137.58, 134.97, 131.07, 128.89, 126.10, 123.71, 123.30, 122.07, 40.17, 34.77, 33.37, 33.21, 32.06, 29.81, 29.03, 26.77, 25.38, 23.19, 22.84, 14.28, –8.13. Anal. Calcd for $\text{C}_{56}\text{H}_{78}\text{S}_6\text{Sn}_2$: C, 56.95; H,

S, 16.29. Found: C, 56.87; H, 6.59; S, 16.20. MALDI–MS: calcd, m/z = 1180.2; found, 1181.1 [M^+].

2,6-Bis(trimethyltin)-4,8-bis(5'-(2-butyloctyl)-[2,2';5',2"-terthiophen]-5-yl)benzo[1,2-b:4,5-b']dithiophene (BDT-T3). A dark yellow solid (yield 67%). $^1\text{H NMR}$ (CDCl_3 , 400 MHz), δ (ppm): 7.73 (s, 2H), 7.43 (d, 2H), 7.32 (d, 2H), 7.18 (d, 2H), 7.06 (d, 2H), 7.03 (d, 2H), 6.69 (d, 2H), 2.76 (d, 4H), 1.65 (m, 2H), 1.38–1.22 (br, 32H), 0.95–0.86 (m, 12H), 0.43 (s, 18H). $^{13}\text{CNMR}$ (CDCl_3 , 100 MHz), δ (ppm): 144.47, 143.56, 143.48, 139.30, 138.21, 137.57, 137.51, 135.40, 134.84, 131.01, 129.07, 126.11, 124.69, 123.72, 123.64, 123.55, 121.98, 40.12, 34.74, 33.35, 33.21, 32.06, 29.78, 29.02, 26.75, 23.16, 22.84, 22.69, 14.27, –8.13. Anal. Calcd for $\text{C}_{64}\text{H}_{82}\text{S}_8\text{Sn}_2$: C, 57.14; H, 6.14; S, 19.07. Found: C, 57.06; H, 6.11; S, 19.01. MALDI–MS: calcd, m/z = 1344.2; found, 1345.1 [M^+].

2,6-Bis(trimethyltin)-4,8-bis(5'-(2-butyloctyl)-[2,2';5',2";5",2"-quaterthiophen]-5-yl)benzo[1,2-b:4,5-b']dithiophene (BDT-T4). A brown solid (yield 59%). $^1\text{H NMR}$ (CDCl_3 , 400 MHz), δ (ppm): 7.72 (s, 2H), 7.44 (d, 2H), 7.34 (d, 2H), 7.19 (d, 2H), 7.11 (d, 2H), 7.10 (d, 2H), 7.03 (d, 2H), 7.00 (d, 2H), 6.68 (d, 2H), 2.75 (d, 4H), 1.64 (m, 2H), 1.37–1.21 (br, 32H), 0.94–0.85 (m, 12H), 0.42 (s, 18H). $^{13}\text{CNMR}$ (CDCl_3 , 100 MHz), δ (ppm): 144.47, 143.67, 142.87, 137.18, 136.56, 135.26, 134.76, 134.45, 128.04, 126.09, 124.52, 124.37, 124.17, 124.02, 123.84, 123.71, 123.64, 123.59, 123.52, 123.14, 121.89, 40.10, 34.73, 33.17, 33.03, 32.04, 29.78, 29.00, 26.74, 23.15, 23.01, 22.83, 14.26, –8.10. Anal. Calcd for $\text{C}_{72}\text{H}_{86}\text{S}_{10}\text{Sn}_2$: C 57.29, H 5.74, S 21.21; found: C 57.21, H 5.68, S 21.16. MALDI–MS: calcd m/z = 1508.2; found 1509.1 [M^+].

5,6-Difluoro-4,7-bis(4-(2-ethylhexyl)-2-thienyl)-2,1,3-benzothiadiazole (9). Into a 250 mL flame-dried 3-neck round-bottom flask with a condenser were added 5,6-difluoro-4,7-diiodobenzo[*c*][1,2,5]-thiadiazole (2.1 g, 5 mmol), (4-(2-ethylhexyl)thiophen-2-yl)-trimethylstannane (5.2 g, 11 mmol), $\text{Pd}(\text{PPh}_3)_4$ (120 mg), and dry toluene (80 mL) under nitrogen protection. The reaction mixture was stirred at 105 °C for 48 h and then cooled to room temperature. The crude product was extracted with CH_2Cl_2 (100 mL × 3) and purified by column chromatography with hexane/dichloromethane (95:5) as eluent. The solvent was evaporated and the product was recrystallized from 2-propanol as orange solid (2.12 g, yield 73%) $^1\text{H NMR}$ (CDCl_3 , 400 MHz), δ (ppm): 8.09 (s, 2H), 7.19 (s, 2H), 2.65 (d, 4H), 1.65 (m, 2H), 1.25–1.40 (m, 16H), 0.80–0.94 (m, 12H). $^{13}\text{C NMR}$ (CDCl_3 , 100 MHz), δ (ppm): 151.05, 150.85, 148.81, 148.77, 148.47, 148.27, 142.23, 132.70, 131.03, 124.81, 111.57, 111.48, 40.45, 34.53, 32.56, 29.16, 25.72, 23.06, 14.11, 10.88.

5,6-Difluoro-4,7-bis(5-bromo-4-(2-ethylhexyl)-2-thienyl)-2,1,3-benzothiadiazole (DT2FBT). Compound 7 (1.0 g, 1.91 mmol) and *N*-bromosuccinimide (NBS) (0.74 g, 4.16 mmol) were added into THF under stirring. The reaction mixture was stirred at a room temperature overnight and then washed with brine and dried over MgSO_4 . The solvent was removed under a reduced pressure and an orange solid was obtained by column chromatography using hexane/dichloromethane (9:1) as the eluent. Needle-like crystal was obtained by recrystallization from iso-propanol (1.00 g, yield 77%). $^1\text{H NMR}$ (CDCl_3 , 400 MHz), δ (ppm): 7.93 (s, 2H), 2.61 (d, 4H), 1.72 (m, 2H), 1.25–1.41 (m, 16H), 0.79–0.96 (m, 12H). $^{13}\text{C NMR}$ (CDCl_3 , 100 MHz), δ (ppm): 151.19, 150.99, 148.60, 148.54, 147.93, 141.92, 132.49, 132.44, 131.21, 115.25, 115.25, 111.11, 40.14, 33.90, 32.64, 28.92, 25.87, 23.22, 14.28, 11.01. $^{19}\text{F NMR}$ (CDCl_3 , 100 MHz), δ (ppm): –127.18 (s, 2F). Anal. Calcd: $\text{C}_{30}\text{H}_{36}\text{Br}_2\text{F}_2\text{N}_2\text{S}_3$: C, 50.14; H, 5.05; S, 13.39. Found: C, 50.62; H, 5.07; S, 13.69.

4.3. Synthesis of Polymers. Compounds BDT-Tn monomers (0.5 mmol), DT2FBT monomer (0.5 mmol), $\text{Pd}_2(\text{dba})_3$ (8.5 mg), and $\text{P}(o\text{-tol})_3$ (12.5 mg) were added to a flame-dried and nitrogen-filled 3-neck flask (50 mL). Three nitrogen purge/vacuum cycles under vigorous stirring were done before adding degassed toluene/*N,N*-dimethylformamide (DMF) (10:1, v/v). After stirring at 110 °C for 48 h, trimethylthienyltin (0.15 equiv) was added to the reaction flask and the reaction was kept at 110 °C for an additional 3 h. 2-Bromothiophene (0.5 equiv) was then added to the reaction flask, and the temperature was kept at 110 °C for an additional 5 h to complete the end-capping reaction. The mixture was cooled to room

temperatures and added dropwise to methanol (300 mL) to obtain a precipitate. After stirring for several hours, the resultant polymer was collected by filtration, dried and extracted successively with methanol, acetone, and hexane by using a Soxhlet extraction apparatus to remove oligomers and catalyst residue. The remaining solid was extracted with chloroform or chlorobenzene and then precipitated in methanol. The precipitate was filtered and dried in vacuum at 40 °C overnight.

PBDT2FBT-T1. Dark blue solid (321 mg, 63%). GPC: $M_n = 28.1 \text{ kg mol}^{-1}$, $M_w = 49.3 \text{ kg mol}^{-1}$, PDI = 1.75. ^1H NMR (DCB- d_4 , 500 MHz, 383 K) δ (ppm): 8.50 (s, 2H), 8.20 (s, 2H), 7.69 (s, 2H), 7.18 (s, 2H), 3.21 (m, 4H), 3.12 (m, 4H), 2.14 (m, 2H), 2.04 (m, 2H), 1.7–1.5 (bm, 48H), 1.15 (m, 12H), 1.07 (m, 12H). Anal. Calcd: C₇₂H₉₄F₂N₂S₇: C, 69.18; H, 7.58; N, 2.24; S, 17.96. Found: C, 69.15; H, 7.55; N, 2.17; S, 17.89.

PBDT2FBT-T2. Dark brown solid with a metallic luster (428 mg, 75%). GPC: $M_n = 42.8 \text{ kg mol}^{-1}$, $M_w = 48.6 \text{ kg mol}^{-1}$, PDI = 1.13. ^1H NMR (DCB- d_4 , 500 MHz, 383 K) δ (ppm): 8.48 (s, 2H), 8.22 (s, 2H), 7.73 (s, 2H), 7.46 (s, 2H), 7.29 (s, 2H), 6.90 (s, 2H), 3.21 (m, 4H), 2.99 (m, 4H), 2.14 (m, 2H), 1.94 (m, 2H), 1.75–1.5 (bm, 48H), 1.15–1.06 (bm, 24H). Anal. Calcd: C₈₀H₉₈F₂N₂O₂S₉: C, 67.94; H, 6.98; N, 1.98; S, 20.41. Found: C, 67.91; H, 6.95; N, 1.91; S, 20.56.

PBDT2FBT-T3. Dark blue solid (321 mg, 63%). GPC: $M_n = 48.2 \text{ kg mol}^{-1}$, $M_w = 102.1 \text{ kg mol}^{-1}$, PDI = 2.11. ^1H NMR (DCB- d_4 , 500 MHz, 383 K) δ (ppm): 8.48 (s, 2H), 8.23 (s, 2H), 7.77 (s, 2H), 7.50 (s, 2H), 7.32 (s, 2H), 7.19 (s, 4H), 6.88 (s, 2H), 3.22 (m, 4H), 2.95 (m, 4H), 2.15 (m, 2H), 1.91 (m, 2H), 1.74–1.49 (bm, 48H), 1.17–1.07 (bm, 24H). Anal. Calcd: C₈₈H₁₀₂F₂N₂S₁₁: C, 66.96; H, 6.51; N, 1.77; S, 22.35. Found: C, 66.87; H, 6.48; N, 1.76; S, 22.32.

PBDT2FBT-T4. Dark blue solid (346 mg, 72%). GPC: $M_n = 33.8 \text{ kg mol}^{-1}$, $M_w = 115.1 \text{ kg mol}^{-1}$, PDI = 3.40. ^1H NMR (DCB- d_4 , 500 MHz, 383 K) δ (ppm): 8.47 (s, 2H), 8.24 (s, 2H), 7.79 (s, 2H), 7.53 (s, 2H), 7.32 (s, 2H), 7.21 (s, 4H), 7.16 (s, 4H), 6.86 (s, 2H), 3.23 (m, 4H), 2.94 (m, 4H), 2.15 (m, 2H), 1.91 (m, 2H), 1.70–1.45 (bm, 48H), 1.17–1.07 (bm, 24H). Anal. Calcd: C₉₆H₁₀₆F₂N₂O₂S₁₃: C, 66.16; H, 6.13; N, 1.61; S, 23.92. Found: C, 66.21; H, 6.15; N, 1.63; S, 23.97.

4.4. Fabrication and Characterization of Organic Solar Cell.

Indium tin oxide (ITO)-coated glass substrates were cleaned sequentially with detergent, distilled water, acetone, and isopropyl alcohol. For photovoltaic devices with a MoO₃ interlayer, a MoO₃ film (9 nm) was thermally evaporated with a rate of 0.1 nm s⁻¹ on UV-treated ITO substrates. PBDT2FBT-Tn and PC₇₁BM were dissolved in CB or DCB with various weight ratios and the blend solutions were kept at a high temperature (90 °C) for more than 12 h. The PBDT2FBT-T1:PC₇₁BM blend solutions were readily dissolved in CB or DCB at room temperature, but the PBDT2FBT-T2, -T3, and -T4:PC₇₁BM blend films had to be processed from hot solutions in order to prevent premature aggregation of the polymers. The PBDT2FBT-Tn:PC₇₁BM solutions were spin-coated onto MoO₃-deposited substrates, and then the films were left in a N₂ atmosphere to dry completely. To deposit the electrodes, the samples were transferred into a vacuum chamber (pressure <1 × 10⁻⁶ Torr), and then LiF (0.6 nm)/Al (100 nm) were deposited sequentially in a conventional structure on top of the thin films by thermal evaporation. The architecture of OPV devices was (ITO/MoO₃(9 nm)/PBDT2FBT-Tn:PC₇₁BM/LiF(0.6 nm)/Al(100 nm)) and the device area was 0.055 cm². The electrical characteristics were measured with a source/measure unit (Keithley 4200) in the dark and under 100 mW cm⁻² AM1.5 solar illumination in a N₂-filled glovebox. Light was generated with an Oriel 1 kW solar simulator referenced using a Reference Cell PVM 132 calibrated by the National Renewable Energy Laboratory (NREL). The incident photon-to-current conversion efficiency (IPCE) was evaluated using a photomodulation spectroscopy setup (Merlin, Oriel) with monochromatic light from a xenon lamp. The power density of monochromatic light was calibrated using a Si photodiode certified by the National Institute for Standards and Technology (NIST).

ASSOCIATED CONTENT

Supporting Information

Experimental details and characterizations. This material is available free of charge via the Internet at <http://pubs.acs.org>.

AUTHOR INFORMATION

Corresponding Author

(K.C.) E-mail: kwcho@postech.ac.kr

Author Contributions

[†]J.L. and J.-H.K. contributed equally to this work.

Notes

The authors declare no competing financial interest.

ACKNOWLEDGMENTS

This work was supported by a grant (Code No. 2011-0031628) from the Center for Advanced Soft Electronics under the Global Frontier Research Program of the Ministry of Science, ICT and Future Planning, Korea. The authors thank the Pohang Accelerator Laboratory for providing the synchrotron radiation sources at 3C and 9A beamlines used in this study.

REFERENCES

- (1) Yu, G.; Gao, J.; Hummelen, J. C.; Wudl, F.; Heeger, A. J. *Science* **1995**, 270, 1789.
- (2) Arias, A. C.; MacKenzie, J. D.; McCulloch, I.; Rivnay, J.; Salleo, A. *Chem. Rev.* **2010**, 110, 3.
- (3) Denner, G.; Scharber, M. C.; Brabec, C. J. *Adv. Mater.* **2009**, 21, 1323.
- (4) Guo, X.; Zhou, N.; Lou, S. J.; Smith, J.; Tice, D. B.; Hennek, J. W.; Ortiz, R. P.; Navarrete, J. T. L.; Li, S.; Strzalka, J.; Chen, L. X.; Chang, R. P. H.; Facchetti, A.; Marks, T. J. *Nat. Photonics* **2013**, 7, 825.
- (5) Hendriks, K. H.; Heintges, G. H. L.; Gevaerts, V. S.; Wienk, M. M.; Janssen, R. A. *Angew. Chem., Int. Ed.* **2013**, 52, 8341.
- (6) Dou, L.; Chen, C.; Yoshimura, K.; Ohya, K.; Chang, W.; Gao, J.; Liu, Y.; Richard, E.; Yang, Y. *Macromolecules* **2013**, 46, 3384.
- (7) Nguyen, T. L.; Choi, H.; Ko, S.-J.; Uddin, M. A.; Walker, B.; Yum, S.; Jeong, J.-E.; Yun, M. H.; Shin, T. J.; Hwang, S.; Kim, J. Y.; Woo, H. Y. *Energy Environ. Sci.* **2014**, 7, 3040.
- (8) Liu, Y.; Zhao, J.; Li, Z.; Mu, C.; Ma, W.; Hu, H.; Jiang, K.; Lin, H.; Ade, H.; Yan, H. *Nat. Commun.* **2014**, DOI: 10.1038/ncomms6293.
- (9) Cheng, Y. J.; Yang, S. H.; Hsu, C. S. *Chem. Rev.* **2009**, 109, 5868.
- (10) Chen, J.; Cao, Y. *Acc. Chem. Res.* **2009**, 42, 1709.
- (11) Huo, L.; Hou, J.; Zhang, S.; Chen, H.-Y.; Yang, Y. *Angew. Chem., Int. Ed.* **2010**, 49, 1500.
- (12) Ye, L.; Zhang, S.; Huo, L.; Zhang, M.; Hou, J. *Acc. Chem. Res.* **2014**, 47, 1595.
- (13) Mei, J.; Bao, Z. *Chem. Mater.* **2014**, 26, 604.
- (14) Hou, J.; Tan, Z.; Yan, Y.; He, Y.; Yang, C.; Li, Y. *J. Am. Chem. Soc.* **2006**, 128, 4911.
- (15) Zhang, Z.-G.; Li, Y. *Sci. China Chem.* **2015**, 58, 192.
- (16) Zhang, M.; Gu, Y.; Guo, X.; Liu, F.; Zhang, S.; Huo, L.; Russell, T. P.; Hou, J. *Adv. Mater.* **2013**, 25, 4944.
- (17) Ai, L.; Ouyang, X. H.; Liu, Q. D.; Wang, S. Y.; Peng, R. X.; Islam, A.; Ge, Z. Y. *Dyes Pigm.* **2015**, 115, 73.
- (18) Jiang, J.-M.; Lin, H.-K.; Lin, Y.-C.; Chen, H.-C.; Lan, S.-C.; Chang, C.-K.; Wei, K.-H. *Macromolecules* **2014**, 47, 70.
- (19) Zhang, o.; Ye, L.; Zhao, W.; Liu, D.; Yao, H.; Hou, J. *Macromolecules* **2014**, 47, 4653.
- (20) Jiang, J.-M.; Raghunath, P.; Lin, H.-K.; Lin, Y.-C.; Lin, M. C.; Wei, K.-H. *Macromolecules* **2014**, 47, 7070.
- (21) Warnan, J.; Labban, A. E.; Cabanatos, C.; Hoke, E. T.; Shukla, P. K.; Risko, C.; Brédas, J.-L.; McGehee, M. D.; Beaujuge, P. M. *Chem. Mater.* **2014**, 26, 2299.
- (22) Kim, J.-H.; Song, C. E.; Kim, B.; Kang, I.-N.; Shin, W. S.; Hwang, D.-H. *Chem. Mater.* **2014**, 26, 1234.

- (23) Chung, H.-S.; Lee, W.-H.; Song, C. E.; Shin, Y.; Kim, J.; Lee, S. K.; Shin, W. S.; Moon, S.-J.; Kang, I.-N. *Macromolecules* **2014**, *47*, 97.
- (24) Kuo, C.; Huang, Y.; Hsiow, C.; Yang, Y.; Huang, C.; Rwei, S.; Wang, H.; Wang, L. *Macromolecules* **2013**, *46*, 5985.
- (25) Kularatne, R. S.; Taenzler, F. J.; Magurudeniya, H. D.; Du, J.; Murphy, J. W.; Sheina, E. E.; Gnade, B. E.; Biewer, M. C.; Stefan, M. C. *J. Mater. Chem. A* **2013**, *1*, 15535.
- (26) Bolognesi, M.; Gedefaw, D.; Dang, D.; Henriksson, P.; Zhuang, W.; Tessarolo, M.; Wang, E.; Muccini, M.; Serid, M.; Andersson, M. R. *RSC Adv.* **2013**, *3*, 24543.
- (27) Kuo, C.-Y.; Nie, W.; Tsai, H.; Yen, H.-J.; Mohite, A. D.; Gupta, G.; Dattelbaum, A. M.; William, D. J.; Cha, K. C.; Yang, Y.; Wang, L.; Wang, H.-L. *Macromolecules* **2014**, *47*, 1008.
- (28) Meng, K.; Ding, Q.; Wang, S.; He, Y.; Li, Y.; Gong, Q. *J. Phys. Chem. B* **2010**, *114*, 2602.
- (29) Lee, J.; Kim, M.; Kang, B.; Jo, S. B.; Kim, H. G.; Shin, J.; Cho, K. *Adv. Energy Mater.* **2014**, *4*, 1400087.
- (30) Brabec, C. J.; Cravino, A.; Meissner, D.; Sariciftci, N. S.; Fromherz, T.; Rispens, M. T.; Sanchez, L.; Hummelen, J. C. *Adv. Funct. Mater.* **2001**, *11*, 374.
- (31) Zhou, H.; Yang, L.; Stuart, A. C.; Price, S. C.; Liu, S.; You, W. *Angew. Chem., Int. Ed.* **2011**, *50*, 2995.
- (32) Shim, C.; Kim, M.; Ihn, S.; Choi, Y. S.; Kim, Y.; Cho, K. *Chem. Commun.* **2012**, *48*, 7206.
- (33) Kim, J. S.; Fei, Z.; Wood, S.; James, D. T.; Sim, M.; Cho, K.; Heeney, M. J.; Kim, J.-S. *Adv. Energy Mater.* **2014**, 1400527.
- (34) Schroeder, B. C.; Huang, Z.; Ashraf, R. S.; Smith, J.; D'Angelo, P.; Watkins, S. E.; Anthopoulos, T. D.; Durrant, J. R.; McCulloch, I. *Adv. Funct. Mater.* **2012**, *22*, 1663.
- (35) Steyrleuthner, R.; Schubert, M.; Howard, I.; Klaumünzer, B.; Schilling, K.; Chen, Z.; Saalfrank, P.; Laquai, F.; Facchetti, A.; Neher, D. *J. Am. Chem. Soc.* **2012**, *134*, 18303.
- (36) Hou, J.; Chen, H. Y.; Zhang, S.; Chen, R. I.; Yang, Y.; Wu, Y.; Li, G. *J. Am. Chem. Soc.* **2009**, *131*, 15586.
- (37) Becke, A. D. *J. Chem. Phys.* **1993**, *98*, 5648.
- (38) Lee, C. T.; Yang, W. T.; Parr, R. G. *Phys. Rev. B* **1988**, *37*, 785.
- (39) Stephens, P. J.; Devlin, F. J.; Chabalowski, C. F.; Frisch, M. J. *J. Phys. Chem.* **1994**, *98*, 11623.
- (40) Xu, Y.-X.; Chueh, C.-C.; Yip, H.-L.; Ding, F.-Z.; Li, Y.-X.; Li, C.-Z.; Li, X.; Chen, W.-C.; Jen, A. K.-Y. *Adv. Mater.* **2012**, *24*, 6356.
- (41) McCulloch, I.; Heeney, M.; Chabinyc, M. L.; DeLongchamp, D.; Kline, R. J.; Cölle, M.; Duffy, W.; Fischer, D.; Gundlach, D.; Hamadani, B.; Hamilton, R.; Richter, L.; Salleo, A.; Shkunov, M.; Sparrowe, D.; Tierney, S.; Zhang, W. *Adv. Mater.* **2009**, *21*, 1091.
- (42) Park, J. H.; Kim, J. S.; Lee, J. H.; Lee, W. H.; Cho, K. *J. Phys. Chem. C* **2009**, *113*, 17579.
- (43) Tumbleston, J. R.; Collins, B. A.; Yang, L.; Stuart, A. C.; Gann, E.; Ma, W.; You, W.; Ade, H. *Nat. Photonics* **2014**, *8*, 385.
- (44) Huang, Y.; Kramer, E. J.; Heeger, A. J.; Bazan, G. C. *Chem. Rev.* **2014**, *114*, 7006.
- (45) Kim, J.-H.; Kim, M.; Jinnai, H.; Shin, T. J.; Kim, H.; Park, J. H.; Jo, S. B.; Cho, K. *ACS Appl. Mater. Interfaces* **2014**, *6*, 5640.
- (46) Peumans, P.; Yakimov, A.; Forrest, S. R. *J. Appl. Phys.* **2003**, *93*, 3693.
- (47) Slooff, L. H.; Veenstra, S. C.; Kroon, J. M.; Moet, D. J. D.; Sweelssen, J.; Koetse, M. M. *Appl. Phys. Lett.* **2007**, *90*, 143506.
- (48) Jo, J.; Na, S.-I.; Kim, S.-S.; Lee, T.-W.; Chung, Y.; Kang, S.-J.; Vak, D.; Kim, D.-Y. *Adv. Funct. Mater.* **2009**, *19*, 2398.
- (49) Dennler, G.; Forberich, K.; Scharber, M. C.; Brabec, C. J.; Tomis, I.; Hingerl, K.; Fromherz, T. *J. Appl. Phys.* **2007**, *102*, 054516.
- (50) Park, S. H.; Roy, A.; Beaupre, S.; Cho, S.; Coates, N.; Moon, J. S.; Moses, D.; Leclerc, M.; Lee, K.; Heeger, A. J. *Nat. Photonics* **2009**, *3*, 297.
- (51) Liang, Y.; Xu, Z.; Xia, J.; Tsai, S.-T.; Wu, Y.; Li, G.; Ray, C.; Yu, L. *Adv. Mater.* **2010**, *22*, E135.
- (52) He, X.; Gao, F.; Tu, G.; Hasko, D. G.; Huttner, S.; Greenham, N. C.; Steiner, U.; Friend, R. H.; Huck, W. T. S. *Adv. Funct. Mater.* **2011**, *21*, 139.
- (53) Liao, H.; Tsao, C.; Shao, Y.; Chang, S.; Huang, Y.; Chuang, C.; Lin, T.; Chen, C.; Su, C.; Jeng, U.; Chen, Y.; Su, W. *Energy Environ. Sci.* **2013**, *6*, 1938.
- (54) Goodman, A. M.; Rose, A. *J. Appl. Phys.* **1971**, *42*, 2823.
- (55) Mihailescu, V. D.; Xie, H.; de Boer, B.; Koster, L. J. A.; Blom, P. W. M. *Adv. Funct. Mater.* **2006**, *16*, 699.
- (56) Lim, J. A.; Kim, J.-H.; Qiu, L.; Lee, W. H.; Lee, H. S.; Kwak, D.; Cho, K. *Adv. Funct. Mater.* **2010**, *20*, 3292.
- (57) Kim, J. S.; Lee, J. H.; Park, J. H.; Shim, C.; Sim, M.; Cho, K. *Adv. Funct. Mater.* **2011**, *21*, 480.
- (58) Kim, J.-H.; Park, J. H.; Lee, J. H.; Kim, J. S.; Sim, M.; Shim, C.; Cho, K. *J. Mater. Chem.* **2010**, *20*, 7398.
- (59) Lin, C.; Lin, Y.; Li, S.; Yu, C.; Huang, C.; Lee, S.; Du, C.; Lee, J.; Chen, H.; Chen, C. *Energy Environ. Sci.* **2011**, *4*, 2134.
- (60) Kim, D. H.; Park, Y. D.; Jang, Y.; Yang, H.; Kim, Y. H.; Han, J. I.; Moon, D. G.; Park, S.; Chang, T.; Joo, M.; Ryu, C. Y.; Cho, K. *Adv. Funct. Mater.* **2005**, *15*, 77.
- (61) Osaka, I.; Kakara, T.; Takemura, N.; Koganezawa, T.; Takimiya, K. *J. Am. Chem. Soc.* **2013**, *135*, 8834.
- (62) Rivnay, J.; Mannsfeld, S. C. B.; Miller, C. E.; Salleo, A.; Toney, M. F. *Chem. Rev.* **2012**, *112*, 5488.